Study of a surface raft foundation in dry cohesionless soil subjected to dynamic loading

Raj Banerjee[1], Aniruddha Sengupta[2],* and G. R. Reddy[1]

[1]Bhabha Atomic Research Centre, Mumbai 480 005, India
[2]Department of Civil Engineering, Indian Institute of Technology Kharagpur, Kharagpur 721 302, India

In this study, behaviour of a raft foundation in dry cohesionless soil when subjected to dynamic loadings is presented. The numerical model is validated by model tests on shaking table and numerically by a plane strain finite difference program, FLAC 2D. In both shaking table tests and numerical analyses, the raft located in dry Kasai River sand in Kharagpur has been subjected to 10 cycles of equivalent sinusoidal loadings with an amplitude of 0.2412 *g* at a frequency of 2 Hz, which represents an irregular time history of the Loma Prieta Earthquake (1989). The results of the above study in terms of response time histories, bending moment and lateral displacement of the raft have been validated with numerical simulations, and the results are in reasonable agreement with the corresponding experimental findings. A methodology to study the behaviour of a raft foundation subjected to harmonic excitations has been proposed in terms of vertical deformations of the raft foundation in dry sand for a given value of dynamic (or degraded) factor of safety.

Keywords: Dry soil, dynamic loading, numerical analysis, raft foundation, shaking table test.

SIGNIFICANT work has been done on the dynamic performances of shallow foundations, including some pioneering works that have also studied the settlements of shallow building foundations during dynamic/earthquake loadings[1–14]. Omer[15] solved the problems (static and dynamic) of a raft foundation (idealized as a thin plate) resting on elastic foundations using a coupled methodology which involves geometric nonlinearity. The two-parameter foundation model of Winkler–Pasternak is assumed and the effects of its foundation parameters on raft responses have been studied. Ribeiro and Paiva[16] have numerically solved the interaction of raft resting on soil (which may be half space or having a finite thickness on a rigid base), in which the soil is modelled by boundary elements and the raft as a membrane element. The infinite boundary elements are used for the simulation of far-field condition. Mandal and Roychoudhury[17] studied the responses of a rectangular raft foundation under various transient loadings using a coupled finite element and boundary element (FE–BE) approach. Wang et al.[18] presented the Ritz method for settlement analysis of a rectangular thick raft resting on a homogeneous, elastic half-space. They have considered the effects of shear deformation on the bending moments and settlement of a raft foundation. Stokoe et al.[19] has proposed a method for predicting settlements of shallow footings on granular soils. The method is based on field seismic measurements to evaluate the small-strain shear modulus combined with nonlinear normalized ($G/G_{max} - \log\gamma$) relationships determined in the laboratory. The settlements obtained from experiments were predicted from a commercially available finite element program, PLAXIS. Asgari et al.[20] conducted numerical studies on sands which contain fines with relative densities of 30–40% under different surcharge loading on a shallow foundation in FLAC 2D. The effects of strong-motion parameters (peak ground acceleration (PGA)/PGV, etc.) on complex soil–structure interaction were studied. However, most of these studies were on shallow, static-footing foundations. Comparatively few works have been done on the dynamic behaviour of a raft foundation. In view of this, here we present the behaviour of a raft foundation during dynamic shaking.

We conducted, small-scale model studies on a raft foundation resting on dry sand to understand the behaviour of a raft subjected to seismic loadings and to evaluate the suitability of such type of foundation under dynamic loading conditions. The results of the model tests were compared with those from a plane strain finite difference program called FLAC 2D (ref. 21). A simplified method has been also proposed to derive a relationship between the dynamic settlement of a raft foundation and its corresponding factor of safety under dynamic loading conditions for a given raft size, raft thickness and superstructure loadings.

Experimental set-up

The small-scale model studies on a raft subjected to dynamic loadings were performed on a uniaxial shake table, which is a steel table of dimensions 1 m × 1 m and mounted on rails. The payload of the table is 5 tonne and it vibrates only in the horizontal direction (uniaxial). The table is attached to an actuator which has a capacity of 50 kN with a stroke length of ± 100 mm. The actuator is

servo-controlled, which can accept both harmonic and random vibrations with a frequency range 0.1–50 Hz.

We performed experiments on small-scale models rather than on the actual prototype. The model tests were performed in a rigid wall container of dimensions 0.8 m × 0.85 m × 0.6 m (length × breadth × height). The walls of the container are made of plexiglass of 16 mm thickness, so that one can view inside the test set-up. The plexiglass is fixed in frames which essentially consist of steel angles.

While performing a dynamic test on the shake table, the most relevant point under consideration is to replicate the free field conditions present at a site. As the soil in the test chamber is confined in a finite dimension, the boundary effects present in the chamber result in the generation of compression waves which add inaccuracies in the recorded responses.

Some of the past results reported in the literature support the fact that the introduction of foam sheet enables dissipation of energy to some extent[22,23]. This dissipation of energy reflects to a relatively unexplored area of damping in geotechnical engineering by experimental studies known as radiation damping, which is different from material damping of the soil. These researchers have studied the effect of thickness of foam by plotting the response spectra of foam and wall and they have also suggested a upper limit to the thickness of foam by providing a relationship[22,23].

Similar soft materials have been already used by others, while studying the dynamic and soil liquefaction phenomena[23–28]. As the tank walls are rigid in this study, thermocol of 32 mm thickness was pasted on the inner side of the walls to reduce the generation of unwanted waves as well as reflection and refraction of waves.

All the tests conducted in the present study are in 1 g (actual gravity loading) and follow the scaling law proposed earlier by some researchers[29–31]. The density, grain size distribution and strength parameters of the soil used in the present study remain the same as those for the actual (prototype) soil in the field. The scale factor (λ) utilized in the model study to scale down the other parameters is 20. Table 1 displays the 1 g scaling relationships utilized in this study. A 6 m × 6 m prototype square concrete raft foundation of 0.55 m thickness and M20 grade has been modelled by a square raft foundation of dimensions 300 mm × 300 mm × 15 mm (length, breadth and thickness; Figure 1). In the model raft, a square steel wire mesh (chicken mesh) of 3 mm square opening has been used as the reinforcement. The steel wires are of 1 mm diameter. The raft is casted using a nominal mix of 1 : 3 : 6 of ordinary Portland cement, fine sand and coarse aggregates. The size of the coarse aggregates is chosen so that the mix can pass through the steel reinforcement mesh of the raft. After casting, the models are soaked in water and allowed to cure for more than 28 days. Three strain gauges are attached at the bottom of the raft so that the strains along the raft may be measured during dynamic

excitation. The bending moments along the raft are then back calculated from the strain gauge data collected during the tests. Figure 1 shows the model raft along with the attached strain gauges.

Material properties of Kasai River sand

In this study, a local sand from Kasai River in Kharagpur was used. The GSD of Kasai River sand is shown in Figure 2. It is classified as poorly graded sand (SP), according to the Unified Soil Classification System (USCS). The specific gravity of the sand is 2.72. The maximum and minimum dry unit weights are 18.00 and 14.03 kN/m^3 respectively. The uniformity coefficient (c_u) and coefficient of curvature (c_c) of the sand were found to be 2.84 and 0.87 respectively. In the model tests, bulk unit weight of the sand was maintained at 15.7 kN/m^3, with a relative density (D_r) of 48%. The drained direct shear tests were performed on the sand to find its shear-strength parameters. Three tests were performed on the sand at three different confining pressures (0.5, 1.0 and 1.5 kg/cm^2) to find its shear-strength parameters[32]. All the tests were performed at a strain rate of 1.25 mm/min. Figure 3 a shows shear stress versus displacement curves for the three tests. Figure 3 b illustrates the relationship between normal stress and failure shear stress obtained

Figure 1. Model raft along with the strain gauges.

Table 1. The 1 g scaling law

System variables	Geometric scaling factor
Mass density	1.0
Acceleration	1.0
Length	λ
Strain	1.0

from the tests. A best-fit straight line is obtained, which is a relationship between shear stress and normal stress as given by Mohr–Coulomb failure criteria. The intercept of this line on the Y-axis gives the effective cohesion (c') and slope of the line gives the effective angle of friction (φ'). The shear-strength parameters of the sand (viz. c' and φ') were found by drained shear tests to be 0.0 and 32° respectively. Previous studies have shown that shear wave velocity (or shear modulus) of sand increases with depth because of an increase in the confining pressure[33,34]. Hence, in this study, a parabolic variation of the shear modulus of Kasai River sand, as given below, has been assumed[21]

$$G_0 = p_{ref} K_G \left(\frac{p'}{p_{ref}} \right)^n, \tag{1}$$

where p_{ref} is the reference pressure (100 kPa), p' the mean effective stress, K_G is a stiffness multiplier (133.26, in the present case) and n is an exponent parameter (0.45 in this case). The values of p_{ref} and K_G were obtained from the drained triaxial tests on the sand. Table 2 shows all the material properties for the foundation sand.

Dry sand only

Initially, the tank was filled up to 0.55 m height with dry Kasai River sand maintaining a dry density of 1600 kg/m³ (unit weight = 15.7 kN/m³). Two accelerometers were placed, one on top of the soil and the another on the shake table. The 32 mm thick thermocol sheets were placed between the plexiglass container and sand layer on three sid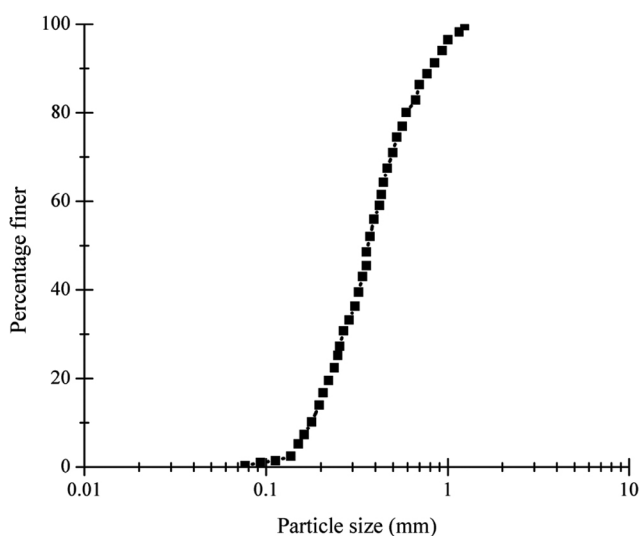es to reduce the reflection of compression/shear waves coming from the tank walls. The bottom of the container was made rough by gluing sand grains at the bottom to allow shear stress at the bottom of the test tank and prevent any slippage[23].

Raft on top of dry sand

In the next experiment, a model raft was placed on top of the sand surface in the middle of the test tank. A vertical surcharge pressure of 1.445 kPa (13 kg load) was applied on top of the model raft. We had to ensure that the vertical surcharge pressure acting on the raft does not cause any bearing capacity failure. The gross allowable bearing pressure (taking a factor of safety equal to 3.0)[35] was found to be 16.64 kPa, which was less than the surcharge loading on the raft. Hence the foundation was statically safe. This surcharge pressure is equivalent to 28.9 kPa in the prototype scale and represents the vertical load of a single-bay, three-storied building.

The inertia of the box is also a contributing factor for the response acceleration at any depth of the soil. The measured accelerations will be less than the actual values, if the box inertia is accounted for[23,26]. Hence, a correction factor for the measured accelerations, expressed as $(m_1 + m_2)/m_1$, has been proposed by Lombardi and Bhattacharya[23], where m_1 is the mass of the soil within the tank and m_2 is the mass of the tank. It is found that the mass of the tank (or the test container) is less than the soil mass by a significant amount; hence the correction factor tends to be unity and thus no correction is done in the present case for the measured accelerations. Figure 4 *a* and *b* shows the top view and schematic diagram of the test set-up with the raft placed on the sand layer within the test chamber.

Selection of input motion

The performance of the Kasai River sand was studied for a PGA of 0.24 g. The catchment area of the river has a number of faults in close proximity, like the Pingla Fault, Garhmayna Khandaghosh Fault and Eocene Hinge Zone[37], due to which mild shakings in this area have occurred a number of times in the past. The area comes under Seismic Zone 3 according to the seismic zonation


Figure 2. Grain size distribution of Kasai River sand from Kharagpur.

Table 2. Geotechnical parameters of sand

Parameters for foundation sand	Value
Mass density (kg/m³)	1600
Cohesion (c'; Pa)	0
Angle of internal friction (φ')	32°
Stiffness multiplier (K_G)	133.26
Exponent (n)	0.45
Poisson's ratio (ν)	0.3
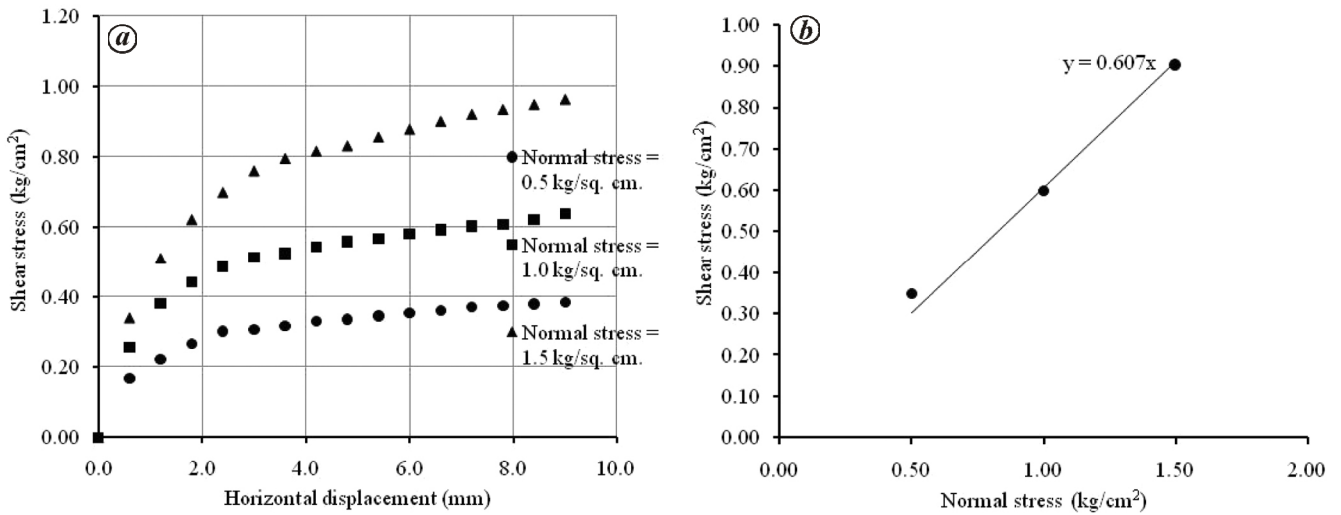
Figure 3. (*a*) Plots of shear–stress versus horizontal displacement curves and (*b*) failure shear stress versus normal stress for three different vertical stresses in a direct shear test.
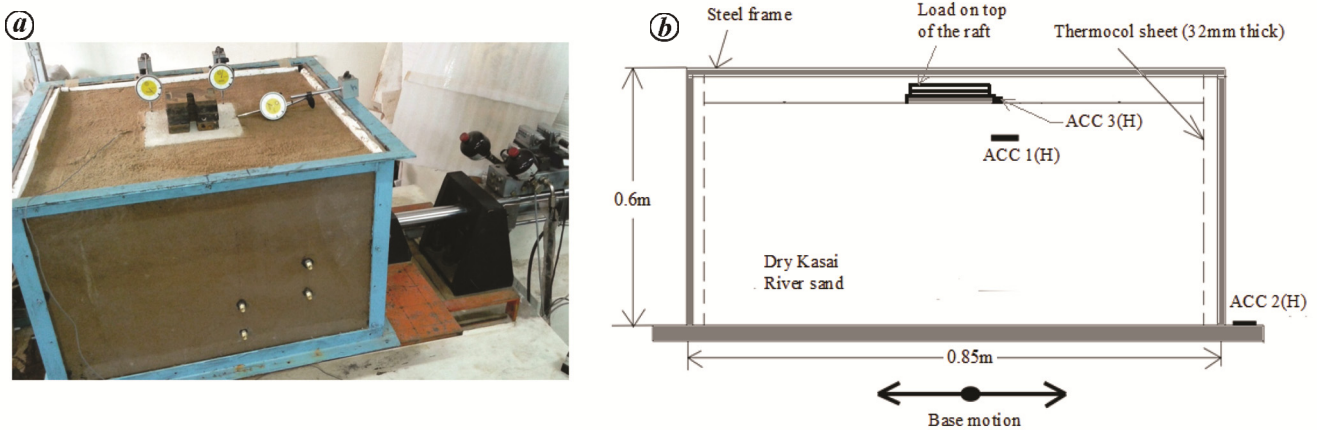
Figure 4. (*a*) Experimental set-up and (*b*) schematic view with the raft on top of dry sand.
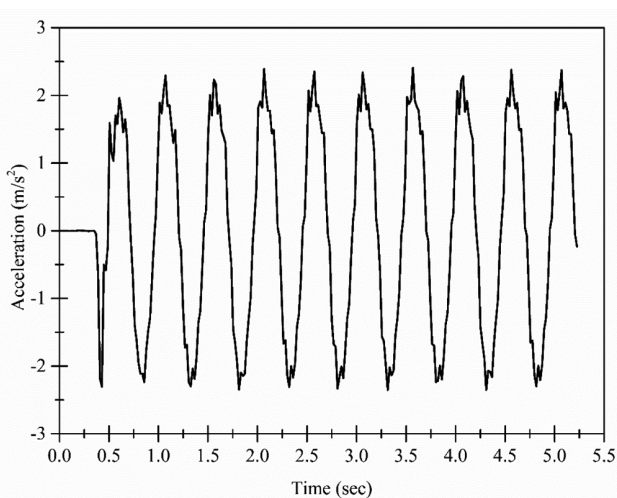
Figure 5. Input motion applied during a shake table test (ACC 2(H)).

map of India[38] and 0.24 g is found to be the maximum possible PGA. Several strong ground motions were analysed and the 18 October 1989 Loma Prieta Earthquake ($M_w = 7.1$, N0W component) motion was chosen for this study. The PGA, v_{max}, d_{max}, and predominant period were 344.17 cm/s^2, 33.339 cm/s, 6.707 cm and 0.607 s (1.67 Hz) respectively, for the selected motion. It is known that the dynamic stresses and the accelerations are inter-related; hence we can replace the actual strong motion by an equivalent harmonic motion consisting of a number of stress cycles of constant amplitude, as proposed by Seed et al.[39]. The strong motion is modelled by 10 cycles of harmonic motion with an amplitude, a_{avg} (two-thirds of PGA) of 0.24 *g* and at a frequency of 2 Hz. The selected acceleration time history is applied at the base of the shake table at a time interval of 0.01953 sec, as shown in Figure 5.

Free vibration characteristics of Kasai River sand

Quite often, the dynamic properties of the soil are identified by allowing it to vibrate freely, which leads to gradual reduction in the amplitude of the vibration. This reduction in wave amplitude is due to the combined effect of radiation damping of the system and material damping of the soil. By closely observing the free vibration response of the soil, one can obtain the natural frequency of vibration as well as overall damping in the system, which includes material as well as radiation damping of the soil. Hence, natural frequency of the soil column is found experimentally from the free-vibration portion of the accelerometer readings near the top surface of the sand bed (Figure 6). Figure 7 *a* shows a close view of the free vibration portion of the motion. Figure 7 *b* shows the accelerometer readings in the frequency domain from where the natural frequency of the soil is obtained. From Figure 7 *b* it may be observed that the natural frequency of the sand is around 10.67 Hz. The damping ratio of the sand is found from the free vibration portion of the response acceleration time history as given below[40,41]

$$\ddot{u}(t) = \pm A \exp(-2\pi f_n t \xi), \tag{2}$$

where f_n is the natural frequency of the sand (10.67 Hz) which is identified from the Fourier spectrum of the free vibration portion and ξ is the damping ratio of the sand.

Therefore, approximating the decay by eq. (2), the damping ratio of the sand is found to be around 4.47% (Figure 7 *a*).

Experimental observations

Dry sand only

For the first model test, where only the sand bed was subjected to dynamic loading, the response acceleration
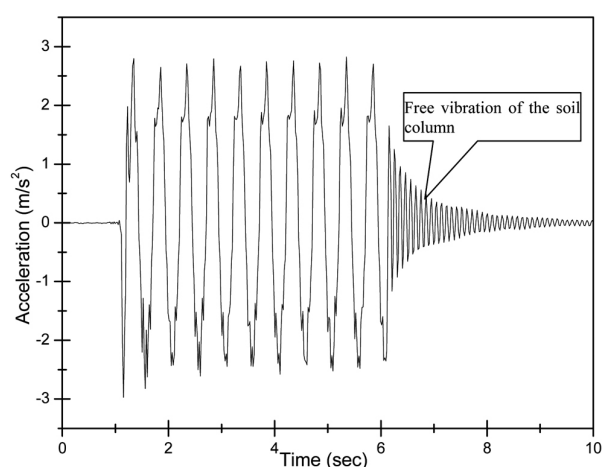
Figure 6. Acceleration time-history at the top of dry Kasai River sand (ACC 1(H)).

history at the top of the sand in dry condition was measured. The amplification of the PGA was calculated by taking the ratio of the measured maximum (absolute) value of acceleration from the top and bottom response histories. The amplification factor was 1.24 for the dry sand.

Raft on top of dry sand

In the second model test, a raft was placed on top of the dry sand and behaviour of the raft under dynamic conditions was studied. The acceleration time history at the top of the sand in dry condition was measured and PGA amplification was found to be 1.20, which is a little less than the value for free field amplification. During the test, strains along the length of the raft were measured by strain indicators. From the strain gauge values, curvature of the raft was calculated. From the curvature equation, moments along the raft were calculated using the well-known relationship for a beam, $M = EI/r$, where E is the modulus of elasticity of the raft, I the moment of inertia of the raft and r is the radius of curvature of the raft given by ε/y. ε is the strain gauge reading and y is the distance of the extreme fibres from the neutral axis. An additional accelerometer was placed on the side of the raft to measure its lateral displacement with time.

Numerical simulation

Two-dimensional finite difference analysis of the model raft foundation, tested on the laboratory shake table, was conducted in FLAC 2D (ref. 21). The 300 mm × 300 m × 15 mm prototype model of the square concrete raft foundation is numerically discretized by 14 two-dimensional beam elements. A beam element has three degrees of freedom (two displacements and one rotation) at each node. The beam elements are assumed to be elastic. The locations of the side and bottom boundaries with respect to the raft in the numerical analyses were chosen to satisfy the actual dimensions of the sand bed in the shake table model tests. The sand bed in the foundation (0.85 m width and 0.55 m height), within which the raft is located, was discretized by 45 × 25 numbers of four-noded plane strain quadrilateral elements of size 0.022 m × 0.022 m. The walls of the test tank were not modelled numerically. In static analysis, the soil–structure system was equilibriated under gravity loads, keeping the bottom nodes of the soil boundary fixed in both directions (*x* and *y*), and the side boundaries fixed in the horizontal (*x*) direction only. It may be noted that during static analysis, the flow calculation option in the program was turned-off, as no water was involved in these tests and the sand was in dry condition.

After performing the initial static analysis, dynamic analysis was performed. In dynamic modelling, it must be
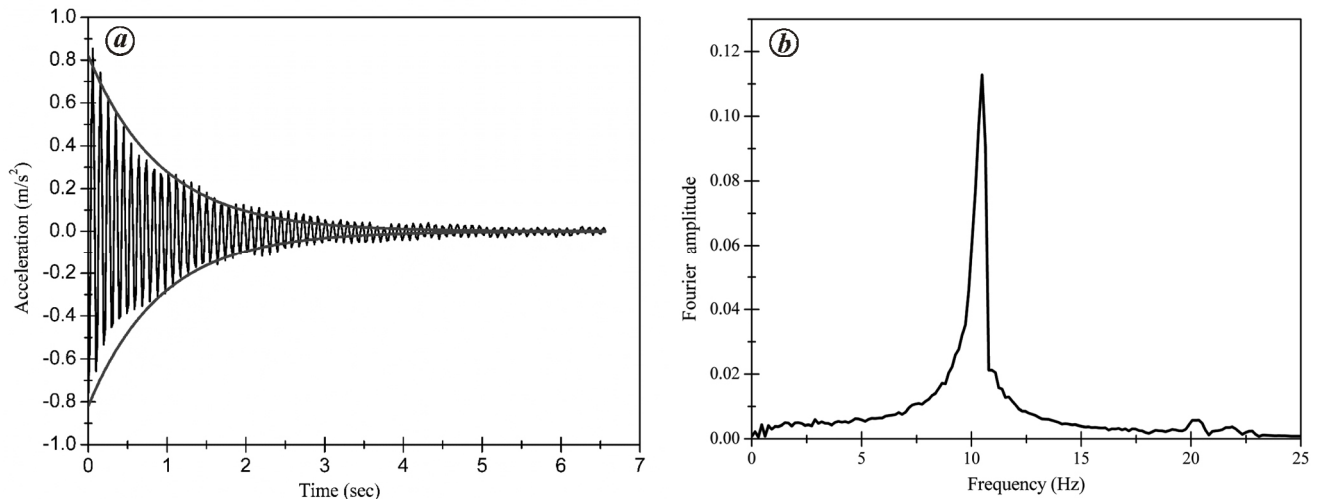
Figure 7. (*a*) Enlarged view of the free vibration portion of acceleration time history and (*b*) acceleration time history in the frequency domain.
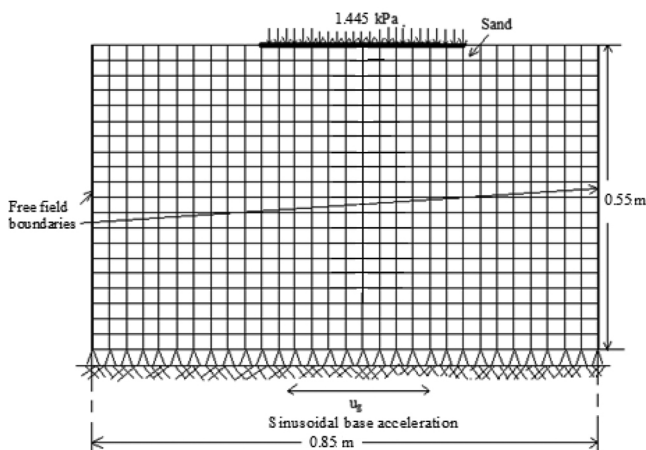
**Figure 8.** Mesh discretization of the raft resting on a sand bed.

ensured that wave propagation through the soil medium is captured adequately. This is done by ensuring that the grid size is small enough to capture the entire wavelength of the shear wave for the desired frequency. In general, minimum three points (or grids) are required to capture a harmonic wavelength of a particular frequency. Hence, corresponding to the grid dimensions, maximum frequency of the wave which can be captured was determined using the following equation[42]

$$ f = \frac{V_s}{10\Delta l}, \qquad (3) $$

where V_s is the shear wave velocity of the sand and Δl is the largest grid size in the numerical model (0.022 m). The numerical value 10 implies that the entire harmonic wavelength of a shear wave of maximum frequency (f) can be captured by 10 number of points (grids). For dynamic analysis, the free field conditions were applied

along the vertical boundaries so that the boundaries retain their non-reflecting properties when subjected to outward propagating waves from the soil structure. The lateral boundaries of the main grid were connected to the free field grid by viscous dashpots to simulate the quiet boundary conditions as developed by Lysmer and Kuhlemeyer[43]. The acceleration time history, given by Figure 5 and applied to the shake table in the laboratory model tests, was applied at the bottom of the soil domain. The magnitude of the maximum acceleration was 2.366 m/s² (0.2412 g). Figure 8 is a schematic diagram illustrating the numerical models (raft and soil) and boundary conditions. In all the numerical analyses, a surcharge load of 1.445 kPa acts vertically on top of the raft. The soil behaviour under dynamic loading is described by an nonlinear elastic-perfectly plastic soil model, which is bascially a Mohr–Coulomb failure criterion coupled with hysteretic behaviour available in FLAC 2D[21].

The reason for adopting this model is because not only does it consider the shear-induced volumetric strain (dilation or contraction)[44] during analysis, but it also takes care of the fact that shear strength of the soil is not underestimated or overestimated at shear strains >1%. While the static properties such as shear strength are measured at shear strains well above 1% (generally 3–5%), we must make sure that the dynamic and static methodologies must be able to produce realistic estimates of the stress–strain behaviour of the soil[45]. If we take the simple nonlinear case which models nonlinear hysteretic damping by in-built 'sigmoidal' models, the drawback is that it underestimates the shear strength of the soil at strains >1%, which is explained subsequently. Four-plane strain, four-noded quadrilateral element of the same dimension as that of the shear box test (i.e. 6 cm width and 4 cm height) was chosen. The soil was subjected to a
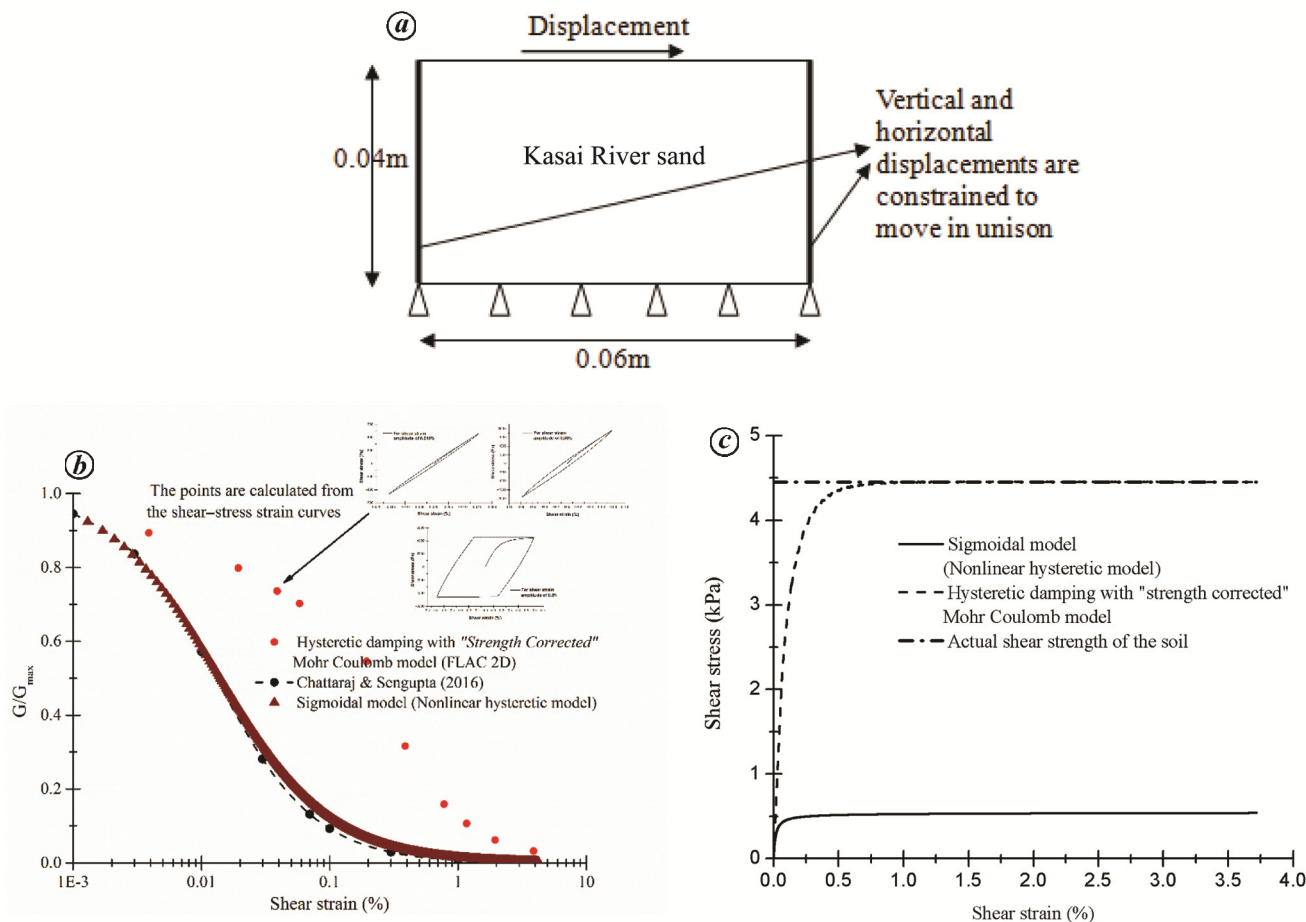
Figure 9. *a*, A single element along with the boundary conditions. *b*, Strength degradation curves for Kasai River sand. *c*, Shear stress versus strain plots for two different models.

vertical stress of 8.73 kPa on top face of the model and allowed to equilibrate under gravity loading, keeping the side boundaries of the soil on roller and bottom boundaries fixed in both directions. This ensures that the mean stress on the soil element is 5.7 kPa, for which the shake table test has been simulated. As it is a drained test, the bulk modulus of water was kept as 0.0 kPa in this simulation. In the next stage, a monotonically increasing displacement of amplitude 3 mm was applied on the top nodes of the soil element. The soil side boundaries were modelled in such a way that they moved in pure shear (vertical deformation of the top nodes were not restricted, but are constrained to move in an identical manner). Figure 9 *a* shows the element along with its boundary conditions. As the shear strains were greater than 0.1% or more, we opted for large strain analysis while predicting the behaviour of the material in the elemental level or simulation of the actual shake table test. In the absence of any simple shear test data for dry Kasai River sand, it is assumed that the cyclic soil behaviour used for modelling the nonlinearity and shake down of the strength of the foundation Kasai River sand during dynamic loading

conditions follow the relationship proposed by Chattaraj and Sengupta[46]. They have reported degradation curves for confining pressures of 50, 100, 200 and 400 kPa, but in this study the mean confining pressure was around 5.7 kPa for which the curves need to be obtained. Hence, the theoretical G/G_0 curves proposed by Menq[47] were fitted with the experimentally obtained values of Chattaraj and Sengupta[46] for different confining pressures. Menq[47] proposed an analytical expression for the estimation of cyclic strength degradation of sand with several curve-fitting parameters which are applicable for Kasai River sand as shown below:

$$\frac{G}{G_0} = \frac{1}{\left(1 + \dfrac{\gamma}{\gamma_{\text{ref}}}\right)^a},$$ (4)

where

$$\gamma_{\text{ref}} = A_\gamma \left(\frac{\sigma'_m}{P_a}\right)^{n_\gamma} \quad \text{and} \quad a = 1.24 + 0.1 \log\left(\frac{\sigma'_m}{P_a}\right).$$

The constant parameter A_γ is estimated as $0.07C_u^{-0.5}$ where C_u is the coefficient of uniformity (2.84 in this study) and the exponent n_γ is estimated as $0.5C_u^{-0.15}$ for Kasai River sand. Equation (4) was used for estimating the degradation curve for Kasai River sand at a confining pressure of 5.7 kPa, which was an input of the hysteretic behaviour ('sigmoidal' model) in the numerical simulation. These curves were fitted with the 'sigmoidal' functions which are well suited for representing modulus degradation curves, because these curves have reasonable asymptotic behaviour at large strains. The 'sigmoidal' model in FLAC 2D (namely, sig3) is defined as follows

$$M_s = \frac{a}{1 + \exp\left(\frac{-(L - x_0)}{b}\right)}, \tag{5}$$

where the logarithmic strain, $L = \log_{10}(\gamma)$, while a, b and x_0 are the curve fitting parameters having values of 1.014, –0.4392 and –1.864 respectively.

Two cases were simulated, one in which the simple 'sigmoidal' hysteretic damping model was used (as described above), which provides hysteresis behaviour (loading/unloading paths are different) in the elastic range, but it does not simulate the actual yield strength of the soil at higher strains. In another case, 'sigmoidal' hysteretic damping was used with an elastic/plastic model. This model is a combination of sigmoidal hysteretic damping with a Mohr–Coulomb model, which implies that the model can simulate actual yield strength of the soil at higher strains. The Mohr–Coulomb model has a constant, tangent, elastic shear modulus, G_{max}, and a constant yield stress. The sigmoidal model has been used to provide energy dissipation in the elastic range[21]. The curve fitting parameters used in the sigmoidal model were 1.014, –0.9592 and –0.464. Figure 9 b shows the modulus reduction curves for the two approaches along with the values predicted by Menq[47] for the confining pressure of 5.7 kPa. The shear stress (τ) and shear strain (γ) relationship can be expressed as follows

$$\frac{\tau}{G_0} = \frac{G_s(\gamma)}{G_0}\gamma = M_s(\gamma)\gamma, \tag{6}$$

where G_s is the strain-dependant shear modulus and a function of γ, G_0 the small-strain modulus ($= \rho V_s^2$), M_s the normalized secant shear modulus (or modulus decay curve with shear strain), ρ the mass density of the soil, γ the shear strain of the soil and V_s is the initial shear wave velocity of the soil. The small-strain shear modulus G_0 of the soil for a particular confining pressure can be obtained from eq. (1). Figure 9 c shows the stress–strain curve obtained for monotonic loading following the two approaches. From the stress–strain curve, one can see the appropriateness for usage of the nonlinear elastoplastic

model for predicting dynamic behaviour of the foundation on the soil, because it preserves the actual soil strength at higher strains; hence this justifies the choice of our soil model. In the numerical computation of raft and soil, the constitutive model was used to update at each calculation step, the tangent shear modulus (M_t) of the nonlinear elastic-perfectly plastic soil model with a Mohr–Coulomb failure criterion using the degradation curve (Figure 9 b).

In this case, the shear strains of different amplitudes were applied to the soil element given in Figure 9 a and the response used to calculate the modulus reduction curve which is plotted in Figure 9 b (red dots). The soil response is given in Figure 9 b (inset) for different values of shear strain. It is to be noted that as the nonlinear elastoplastic model is used to match the peak shear strength of the soil, the soil behaviour will be predicted with less nonlinearity level. The shear modulus degradation level will be such that it predicts stiff behaviour at small to moderate strain levels; but this cannot be avoided because if we use 'sig3' model in FLAC 2D, it is not capable of reaching an asymptotic value of shear stress at high strain levels (Figure 9 c); the same was observed by Hutabarat[48]. The advanced numerical curve fitting techniques developed by Groholski et al.[49] has the ability to capture shear strength of the soil at large strains as well as preserve the small-strain behaviour. However, this technique is not implemented in FLAC 2D and hence cannot be used here. To suppress the high-frequency noise in the obtained acceleration time history, 0.2% Rayleigh damping has been added to hysteretic damping of the soil. The interaction between soil and structure is simulated via nonlinear normal and shear springs connecting each node of the structure and soil. This simulates the relative lateral and downward movement between the soil and structure due to various loadings. The interface parameters which are the normal and shear stiffness were estimated from the drained friction angle (φ'), bulk modulus (K) and shear modulus (G) of the foundation soil[21,50]. In this study, the values were 9.20×10^8 Pa/m in both normal and tangential directions. The cohesion and friction angle of the interface material were 0.0 and 25° respectively.

Results

For the case where only the soil (without the raft on it) was subjected to dynamic loading, the experimentally obtained acceleration time history at the top of the sand layer was compared with the corresponding values from the numerical analysis in both time and frequency domain (Figure 10 a and b respectively). It may be seen from the figure that the accelerations predicted by the numerical study match closely with the experimental observations although there are slight differences which may be due to
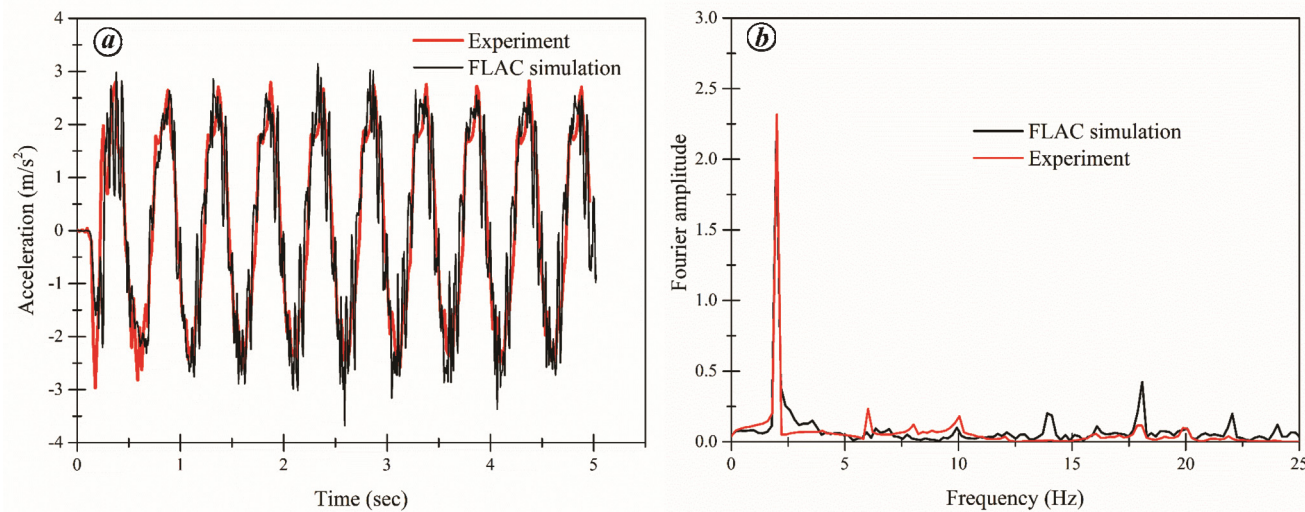
Figure 10. Comparison between experimentally and numerically obtained acceleration time history (*a*) and frequency domain (*b*), for dry sand near the top surface.
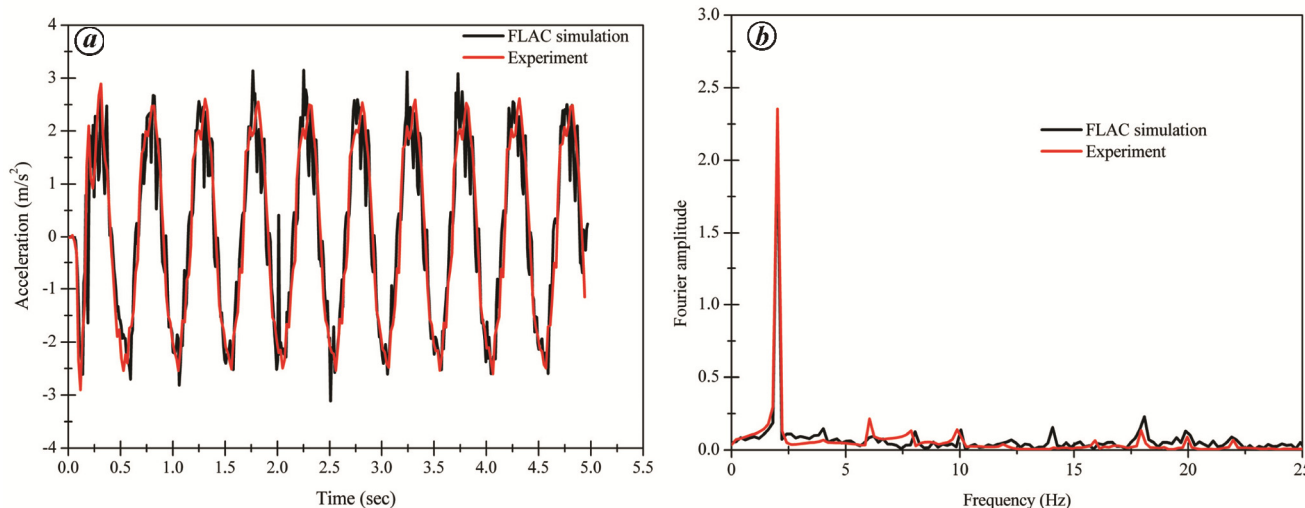
Figure 11. Comparison between experimentally and numerically obtained acceleration time histories (*a*) and frequency domain (*b*) for dry sand near the bottom of the raft.

the selection of mesh size and time step in the numerical analysis.

For the case of a raft on top of the dry sand, the experimentally obtained response time history at the top of the sand was compared with that obtained from the numerical study and shown in both time and frequency domain (Figure 11 *a* and *b*) respectively. The experimental observations match reasonably well with the results obtained from the numerical study. Figure 12 shows a comparison between the experimentally and numerically obtained bending moments in the raft at the end of the dynamic loading. It may be observed that the bending moments calculated by FLAC 2D are in reasonably close agreement with those obtained from the laboratory model tests. The lateral deformation time history of the raft was also

verified (Figure 13). It is seen that the numerical predictions are reasonably close to the experimental observations.

Correlation between dynamic settlements and degraded factor of safety

In the present study, the correlation between the settlement observed at the end of dynamic loading with the dynamic degraded factor of safety (FS_{deg}) was evaluated independently for the prototype raft foundation of M20-grade and $6\,m \times 6\,m$ raft size. The raft was subjected to various vertical loadings ranging from 30 to 60 kPa, and the study was conducted for 0.55 m thick prototype raft (Figure 14). The allowable limit of the dynamic

settlement is not a unique value, but depends on the serviceability requirements of various types of superstructure resting on it. The dynamic degraded factor of safety (FS_{deg}) depends upon the loading and soil strength parameters, which are the average foundation pressure and shear strength of the underlying sand layer. On the other hand, the dynamic settlement (S_{dyn}) depends upon the characteristics of base excitation, which are peak acceleration, a_{max}, peak velocity, v_{max} (or the predominant excitation period, T) and the number of significant loading cycles (N) as well as the foundation bearing pressure. Thus the definition of a factor of safety relates to the static loading ratio[51]

$$\frac{q}{q_{ult}} = \frac{1}{FS_{deg}}.$$

Hence we made an effort to relate S_{dyn} with one composite variable (FS_{deg}) which takes into account all the other
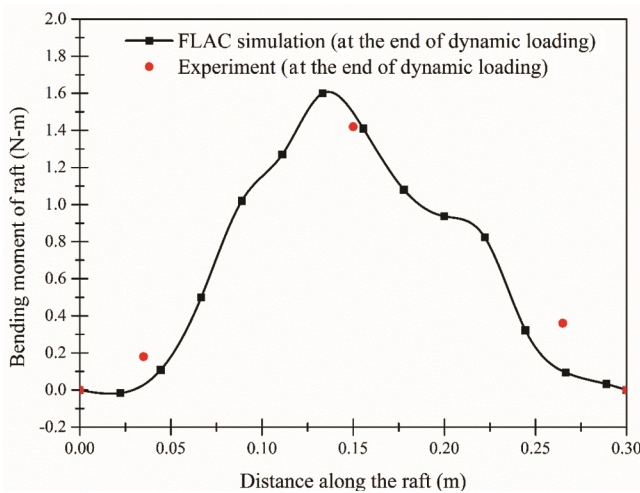
Figure 12. Comparison between experimentally and numerically obtained bending moments in the raft at the end of dynamic loadings.
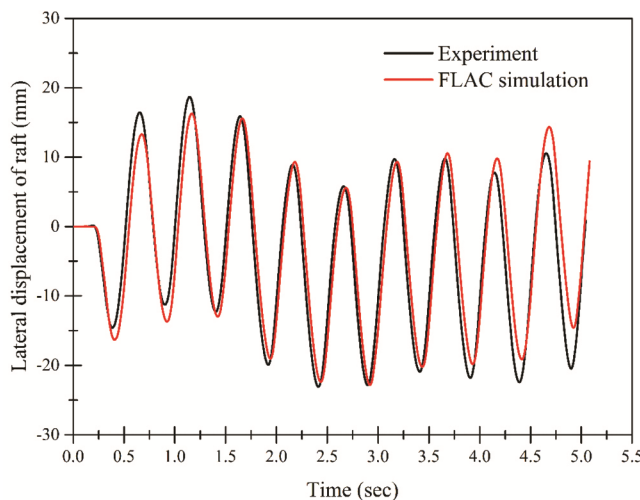
Figure 13. Comparison between experimentally and numerically obtained lateral displacement time histories of the raft.

factors under consideration for a raft resting on dry sand, whose properties are given in Table 2. The dynamic foundation settlements were considered proportional to the term $a_{max}T^2N$, as for a sinusoidal excitation, $a_{max}T^2$ is equivalent to the v_{max}^2/a_{max} term (ref. 52) used in the relationship for the evaluation of dynamic settlement of the raft resting on dry sand[6].

The variation in shear modulus of the sand deposit was obtained from eq. (1). In this case, p_{ref} is the reference pressure (100 kPa), p' is the mean effective stress and K_G is the stiffness multiplier (133.26).

The natural frequency of the sand column was obtained from the following relationship[52]

$$f_n = \frac{(2n-1)V_s}{4H}, \tag{7}$$

where f_n is the natural frequency of the sand, n the mode number (1.0 in the present case), V_s the shear wave velocity of the sand $(G/\rho)^{1/2}$ and H is the height of the sand column (11.0 m in the present case). For finding out the natural frequency of a non-homogeneous profile, the soil profile was divided into 11 layers, each of depth 1 m. The shear modulus of the soil within each layer was taken as the average of the top and the bottom shear modulus values within that layer, and natural frequency of the soil deposit was obtained from the revised relationship as follows[52]

$$V_s = \frac{H}{\sum_{i=1}^{4} \frac{h_i}{V_{si}}}. \tag{8}$$

The natural frequency obtained from eq. (8) for the fundamental mode was found to be 1.70 Hz.

To obtain the correlation between dynamic settlement, S_{dyn} with the degraded factor of safety, 22 analyses for the raft foundation were conducted for sinusoidal excitations of N (number of cycles) varying from 15 to 20, and a_{max} varying from 0.05 to 0.25 g with frequency between 3 and 4 Hz for superstructure loading of 30–60 kPa on top of the raft. All the acceleration records were baseline corrected[53–56] and applied to the bottom nodes of the numerical model. The soil domain was 17 m wide and 11 m
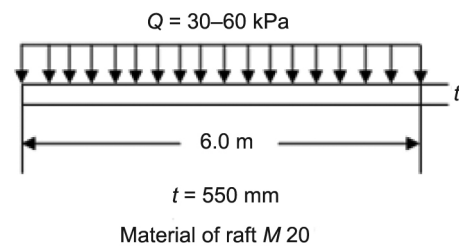
**Figure 14.** Raft of 6 m size with a thickness of 550 mm.

deep. The cyclic soil behaviour of Kasai River sand has been represented by the relationship between M_s and γ given by eq. (5) for a mean confining pressure of 113.81 kPa. For simulating the hysteretic behaviour of sand in the model, the modified curve-fitting parameters a, b and x_0 for the 'sigmoidal' model were 1.014, –0.3892 and –1.304 respectively. To suppress the high-frequency noise in the obtained acceleration time history, 0.2% Rayleigh damping was added to hysteretic damping of the soil. The extent of soil domain is the scaled-up dimensions of the shake table. The raft is made of concrete of M-20 grade with the modulus of elasticity E = $5000\sqrt{f_{ck}}$ (MPa) (IS 456)[54]. In the numerical model, element size was taken to be 0.2 m × 0.2 m and maximum frequency that the grid can capture was found to be around 25 Hz, according to eq. (3). This covers a frequency range wide enough for the concerned structure and soil domain. The value of the interface normal and shear stiffness for soil–structure interaction of the raft was taken to be 5.96×10^8 Pa/m for the analysis. The cohesion and friction angle of the interface material were 0 and 25° respectively.

The values of dynamic settlements with the sinusoidal base excitations were normalized against $a_{max}T^2N$ and plotted against $1/FS_{deg}$ (Figure 15). The following approximate relationship has been established for a raft foundation resting on the Kasai River sand

$$\frac{s_{dyn}}{a_{max}T^2N} = 0.78337 \left(\frac{1}{FS_{deg}}\right)^{1.64762}. \tag{9}$$

Rearranging the terms in eq. (9), we get,

$$S_{dyn} = a_{max}T^2N\,0.78337 \left(\frac{1}{FS_{deg}}\right)^{1.64762}. \tag{10}$$
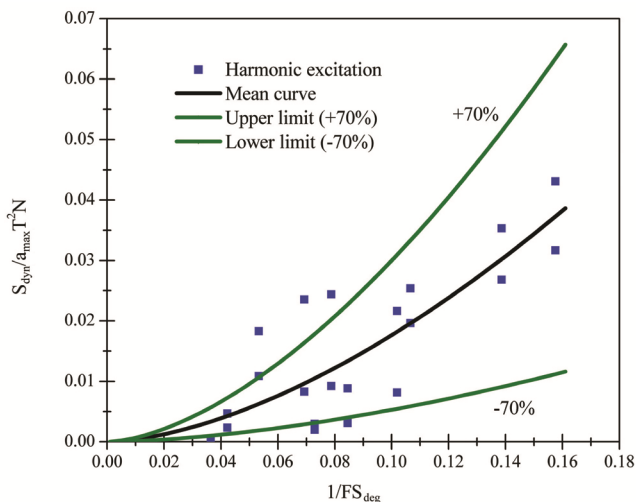
Figure 15. Relationship between degraded factor of safety and seismic settlement for the raft foundation.

The evaluation of dynamic settlement using eq. (10) requires knowledge of post-shaking bearing capacity and degraded factor of safety (FS_{deg}), and is clearly explained by Richards et al.[6].

The ultimate bearing capacity that a strip footing can sustain was estimated according to Terzaghi[56] failure mechanism as

$$q_{ult} = cN_{cE} + qN_{qE} + \frac{1}{2}B\gamma N_{\gamma E}, \tag{11}$$

where $c = 0.0$, $\phi = 32°$ for Kasai River sand. Since the raft lies on the surface, surcharge load, $q = 0.0$ in eq. (11). Therefore, the ultimate bearing capacity for the raft is

$$q_{ult} = \frac{1}{2}B\gamma N_{\gamma E}F_{\gamma S}, \tag{12}$$

where $F_{\gamma s}$ is the shape factor for the raft $(1 - 0.4(B/L); 0.6$ in this study), N_{cE}, N_{qE} and $N_{\gamma E}$ are the seismic bearing capacity factors which depend on the angle of internal friction of the soil and

$$\tan\theta = \frac{k_h}{(1-k_v)}$$

where k_h is the horizontal PGA value applied at the bottom of the soil (0.025, 0.05, 0.1, 0.15, 0.2 and 0.23 in this study) while k_v is the vertical PGA value (0.0 in this study). Table 3 shows the values of seismic-bearing capacity for various levels of ground motion. It should be noted that eqs (9) and (10) proposed are established from 1 g model tests, which suffer from the limitation of confining pressure. The results are for only one relative density of sand. Hence, generalizing the proposed equations is not advisable. In addition, the proposed equations must be revised considering the depth effects (if the raft is embedded in the soil), size of the raft as well as different earthquake loading conditions. However, for 'different earthquake loading conditions', one can convert the actual earthquake into equivalent number of harmonic loading cycles with a reduction of PGA with the predominant frequency of the earthquake, using the method proposed

Table 3. Variation of seismic-bearing capacity for various levels of ground motion

k_h	$N_{\gamma(E)}/N_{\gamma(s)}$	$N_{\gamma(E)}$	q (kPa)
0.025	0.95	28.5548	822.3786105
0.05	0.82	24.6473	709.8425902
0.1	0.65	19.5375	562.680102
0.15	0.5	15.0288	432.8308477
0.2	0.44	13.2254	380.8911459
0.23	0.37	11.1213	320.2948273

by Seed et al.[39]. However, if the strong motion consists of a wide range of frequencies, then there is difficulty in determining a single predominant frequency, in which case the actual strong motion needs to be applied to determine the seismic settlement.

Conclusion

In this study, the dynamic behaviour of a raft foundation resting on top of dry cohesionlesss soil has been analysed using laboratory model tests on shake table and numerically by a plane strain finite difference program[21]. A reasonable match was found between experimental observations and the numerical study. The variations in the results were within tolerable limits. A parametric study has been conducted on the geometry of the raft under sinusoidal harmonic loadings and a simplified methodology for the estimation of dynamic settlements of a square raft foundation resting on dry cohesionless sand has been proposed for a given value of dynamic (or degraded) factor of safety. However, this equation cannot be generalized, because it suffers from limitations in terms of confining pressure, relative density of sand as well as embedment depth of the raft.

1. Richart, F. E., Foundation vibrations. *Trans: ASCE*, 1962, **127**(1), 863–898.
2. Kishida, H., Damage to reinforced concrete buildings on Nigata city with special reference to foundation engineering. *Soils Found.*, 1966, **6**(1), 71–88.
3. Seed, H. B. and Idriss, I. M., Analysis of soil liquefaction: Niigata earthquake. *J. Soil Mech. Found. Div. ASCE*, 1967, **93**(3), 83–108.
4. Richart, F. E. and Whitman, R. V., Design procedures for dynamically loaded foundations. *J. Soil Mech. Found. Div. ASCE*, 1967, **93**(SM6), 168–193.
5. Richart, F. E. and Whitman, R. V., Comparison of footing vibrations with theory. *J. SMFD, Proc. ASCE*, 1967, **93**(SM6), 143–167.
6. Richards, R., Elms, D. G. and Budhu, M., Seismic bearing capacity and settlements of foundations. *J. Geotech. Eng.*, 1993, **119**, 662–674.
7. Yoshimi, Y. and Tokimatsu, K., Settlement of buildings on saturated sand during earthquakes. *Soils Found.*, 1977, **17**(1), 23–38.
8. Dobry, R and Gazettas, G., Dynamic response of arbitrarily shaped foundations. *J. Geotech. Eng. Div. ASCE*, 1986, **112**(2), 109–125.
9. Dobry, R., Gazettas, G. and Stokoe, K. H., Dynamic response of arbitrarily shaped foundations: experimental verification. *J. Geotech. Eng. Div. ASCE*, 1986, **112**(2), 126–154.
10. Gazettas, G. and Stokoe, K. H., Free vibrations of embedded foundations: theory versus experiment. *J. Geotech. Eng. Div. ASCE*, 1991, **117**(9), 1382–1401.
11. Puri, V. K. and Das, B. M., Dynamic response of block foundation. In Third International Conference on Case Histories in Geotechnical Engineering, 1993.
12. Ragheb, A. M., Numerical analysis of seismically induced deformations in saturated granular soil strata. Ph D thesis, Department of Civil Engineering, Rensselaer Polytechnic Institute, NY, 1994.
13. Paolucci, R., Simplified evaluation of earthquake-induced permanent displacements of shallow foundations. *J. Earthq. Eng.*, 1997, **1**(3), 563–579.
14. Gajan, S. and Kutter, B. L., Contact interface model for shallow foundations subjected to combined cyclic loading. *J. Geotech. Geo-Environ. Eng.*, 2009, **135**(3), 407–419.
15. Omer, C., Nonlinear analysis of thin rectangular plates on Winkler–Pasternak elastic foundations by DSC–HDQ methods. *Appl. Math. Modell.*, 2006, **31**, 606–624.
16. Ribeiro, D. B. and Paiva, J. B., An alternative BE–FE formulation for a raft resting on a finite soil layer. *Eng. Anal. Boundary Elem.*, 2015, **50**, 352–359.
17. Mandal, J. J. and Roychoudhury, S., Response of rectangular raft foundations under transient loading. The 12th International Conference of International Association for Computer Methods and Advances in Geomechanics (IACMAG), Goa, 2008.
18. Wang, C. M., Chow, Y. K. and How, Y. C., Analysis of rectangular thick rafts on an elastic half-space. *Comp. Geotech.*, 2000, **28**, 161–184.
19. Stokoe, K. H., Kacar, O. and Van Pelt, J., Predicting settlements of shallow footings on granular soil using nonlinear dynamic soil properties. In Proceedings of 18th International Conference on Soil Mechanics and Geotechnical Engineering, Paris, 2012, pp. 3467–3470.
20. Asgari, A., Golshani, A. and Bagheri, M., Numerical evaluation of seismic response of shallow foundation on loose silt and silty sand. *J. Earth System Sci.*, 2014 **123**(2), 365–379.
21. Itasca, *User's Guide for FLAC Version 5.0*, Itasca India Consulting, Nagpur, 2005.
22. Bhattacharya, S., Lombardi, D., Dihoru, L., Dietz, M., Crewe, A. J. and Taylor, C. A., Model container design for soil–structure interaction studies. *Role of Seismic Testing Facilities in Performance Based Earthquake Engineering, Springer Series*, 2011, vol. 22, pp. 135–158.
23. Lombardi, D. and Bhattacharya, S., Shaking table tests on rigid soil container with absorbing boundaries. Lisbon, 2012, 15WCEE.
24. Banerjee, R., Konai, S., Sengupta, A. and Deb, K., Shake table tests and numerical modeling of Kasai River Sand. *Geotech. Geol. Eng.*, 2017, **35**(4), 1327–1340.
25. Giri, D. and Sengupta, A., Dynamic behaviour of small-scale model of nailed steep slopes. *Geomech. Geoeng.: Int. J.*, 2010, **5**(2), 99–108.
26. Bandyopadhyay, S., Sengupta, A. and Reddy, G. R., Performance of sand and shredded rubber tire mixture as a natural base isolator for earthquake protection. *Earthq. Eng. Eng. Vib.*, 2015, **14**(4), 683–693.
27. Dash, S. R., Lateral pile–soil interaction in liquefiable soils. Ph D thesis, University of Oxford, UK, 2010.
28. Ha, I. S., Olson, S. M., Seo, M. W. and Kim, M. M., Evaluation of reliquefaction resistance using shaking table tests. *Soil Dyn. Earthq. Eng.*, 2011, **31**(4), 682–691.
29. Ramu, M., Prabhu, R. V. and Thyla, P. R., Development of structural similitude and scaling laws for elastic models. *KSCE J. Civil Eng.*, 2011, **17**(1), 139–144.
30. Iai, S., Similitude for shaking table tests on soil–structure–fluid model in 1 g gravitational field. *Soils Found.*, 1989, **29**(1), 105–118.
31. Wood, D. M., Geotechnical Modeling, Version 2.2, 2004.
32. BIS, IS 2720 methods of test for soils, part 13 – direct shear test. Bureau of Indian Standards, New Delhi, 1986.
33. Seed, H. B. and Idriss, I. M., Soil moduli and damping factors for dynamic response analyses. College of Engineering, University of California, Berkeley, USA, 1970.
34. Kawaguchi, T. and Tanaka, H., Formulation of G_{max} from reconstituted clayey soil: its application to measured G_{max} in the field. *Soils Found.*, 2006, **48**, 821–831.
35. Murthy, V. N. S., *Soil Mechanics and Foundation Engineering*, CBS Publishers & Distributors, New Delhi, 2009.
36. Elgamal, A., Yang, Z., Adalier, K. and Sharp, M. K., Effect of rigid container size on dynamic earth dam response in centrifuge

experiments. Proceedings 16th ASCE Engineering Mechanics Conference, University of Washington, Seattle, WA, USA, 2003.

37. Dasgupta, S., Narula, P. L., Acharyya, S. K. and Banerjee, J., *Seismotectonic Atlas of India and its Environs*, Geological Society of India, Kolkata, 2000.

38. BIS, IS 1893 Indian standard criteria for earthquake resistant design of structures, part 1 – general provisions and buildings. Fifth revision. Bureau of Indian Standard, New Delhi, 2002.

39. Seed, H. B., Idriss, I. M., Makdisi, F. and Banerjee, N., Representation of irregular stress time histories by equivalent uniform stress series in liquefaction analysis. EERC-75-29, University of California, Berkeley, USA, 1975.

40. Chopra, A. K., *Dynamics of Structures, Theory and Applications to Earthquake Engineering*, Prentice Hall, 2015, 3rd edn.

41. Chi-Chin, T., Wei-Chun, L. and Jiunn-Shyang, C., Identification of dynamic soil properties through shaking table tests on a large saturated sand specimen in a laminar shear box. *Soil Dyn. Earthq. Eng.*, 2016, **83**, 59–68.

42. Kuhlemeyer, R. L. and Lysmer, J., Finite element method accuracy for wave propagation problems. *J. Soil Mech. Found.*, *Div. ASCE*, 1973.

43. Lysmer, J. and Kuhlemeyer, R. L., Finite dynamic model for infinite media. *J. Eng. Mech.*, 1969, **95**(EM4), 859–877.

44. Vaid, Y. P. and Saitharan, S., The strength and dilatancy of sand. *Can. Geotech. J.*, 1992, **29**(3), 522–526.

45. Griffiths, S. C., Cox, B. R. and Rathje, E. M., Challenges associated with site response analyses for soft soils subjected to high-intensity input ground motions. *Soil Dyn. Earthq. Eng.*, 2016, **85**, 1–10.

46. Chattaraj, R. and Sengupta, A., Liquefaction potential and strain dependent dynamic properties of Kasai River sand. *Soil Dyn. Earthq. Eng.*, 2016, **90**, 467–475.

47. Menq, F. Y., Dynamic properties of sandy and gravelly soils. Ph D dissertation, University of Texas, Austin, USA, 2003.

48. Hutabarat, D., Evaluation of one-dimensional seismic site response analyses at small to large strain level. Thesis (Master's), University of Washington, USA, 2016.

49. Groholski, D. R., Hashash, Y. M. A., Kim, B., Musgrove, M., Harmon, J. and Stewart, J. P., Simplified model for small-strain nonlinearity and strength in 1D seismic site response analysis. *J. Geotech. Geoenviron. Eng.,* 2016, **142**(9), 1–14.

50. Choudhury, S. S., Deb, K. and Sengupta, A., Behavior of underground strutted retaining structure under seismic condition. *Earthq. Struct.*, 2015, **8**(5), 1147–1170.

51. Karamitros, D. K., Bouckovalas, G. D. and Chaloulos, Y. K., Seismic settlements of shallow foundations on liquefiable soil with a clay crust. *Soil Dyn. Earth. Eng.*, 2013, **46**, 64–76.

52. Kramer, S. L., *Geotechnical Earthquake Engineering*, Prentice hall, 1996.

53. Richards, R., Elms, D. G. and Budhu, M., Seismic bearing capacity and settlements of foundations. *J. Geotech. Eng.*, 1993, **119**, 662–674.

54. Yang, J., Li, J. B. and Lin, G., A simple approach to integration of acceleration data for dynamic soil–structure interaction analysis. *Soil Dyn. Earthq. Eng.*, 2006, **26**, 725–734.

55. BIS, IS 456 plain and reinforced concrete code of practice. Fourth revision. Bureau of Indian Standard, New Delhi, 2000.

56. Terzaghi, K., *Theoretical Soil Mechanics*, John Wiley, New York USA, 1943.